The Crystal Structure of $[Cu(HAPH)]ClO_4 \cdot 1.6H_2O$ and the Cleavage of DNA by Analogs of the Metal Binding Core of Bleomycin

REX. E. SHEPHERD*

Department of Chemistry, University of Pittsburgh, Pittsburgh, PA 15260 (U.S.A.)

THOMAS J. LOMIS, RICHARD R. KOEPSEL*

Department of Microbiology/Biochemistry, School of Dental Medicine, University of Pittsburgh, Pittsburgh, PA 15260 (U.S.A.)

RASHMI HEGDE and JEHANGIR S. MISTRY

Department of Medicinal Chemistry, School of Pharmacy, University of Pittsburgh, Pittsburgh, PA 15260 (U.S.A.)

(Received June 17, 1989)

Abstract

An X-ray diffraction study of $[Cu(HAPH)](ClO_4) \cdot 1.61H_2O$ was carried out. The structure of $[Cu(C_{17}H_{20}N_7)](ClO_4) \cdot 1.61H_2O$ was determined for a monoclinic crystal in $C2/c$ with cell constants a = 25.6516(21), b = 8.0478(7), c = 23.624(17) Å, β = 118.114(5)° and Z = 8. The structure was refined to R = 0.064 for 2897 unique observed reflections. The $Cu(HAPH)^+$ cation is a distorted square pyramid with the Cu^{II} center 0.062 Å above the least-squares plane defined by pyridine (N1), amine (N18), deprotonated amide (N9) and imidazole (N13) donors of HAPH; Cu^{II} is displaced toward imidazole (N22). The imidazole (N22) adjacent to the secondary amine serves as the axial donor of the square pyramid. Cu–N distances are as follows: Cu–N1, 1.952(5); Cu–N18, 2.124(5); Cu–N9, 2.013(5); Cu–N13, 1.998(5); Cu–N22, 2.167(6) Å. The in-plane imidazole ring experiences a greater perturbation in the bond between the coordinated N and the 'C4' carbon compared to the axial imidazole.

A 450 base pair restriction fragment of plasmid pT181 DNA and superhelical plasmid pT181 DNA were treated with Fe^{II}(HAPH), Fe^{II}(SAPH-3), Fe^{II}(AMPHIS), $Fe(edta)^{2-}$ and Fe^{II}(BLM). Fe^{II}(BLM) cutting of linear DNA was *c.* ten-fold greater than Fe^{II}(HAPH). The small molecule systems follow the reactivity order Fe^{II}(HAPH) (4×) > Fe^{II}(AMPHIS); Fe^{II}(HAPH) (200×) > Fe^{II}(SAPH-3) or $Fe(edta)^{2-}$. A lack of DNA cleavage fragments derived from cuts at positions 3′ to cytidine bases was noted. Cutting of superhelical plasmid DNA into linear plasmid DNA and further fragmentation was shown to be concentration dependent for Fe^{II}(HAPH).

*Authors to whom correspondence should be addressed.

Introduction

Bleomycins (BLMs) are glycopeptide antibiotics isolated from *Streptomyces verticillus* [1–3]. BLMs exhibit antitumor activity toward Hodgkin's lymphoma and tumors of the head, neck, testis and ovaries. The antitumor action is produced by DNA strand scissions in the presence of Fe^{II}, Co^{II} or Cu^{I} and O_2 [2–6]. The metal ion binding region of BLM is similar to the Cu^{II} binding site of human serum albumin [2], but BLM has an additional axial ligation absent in serum albumin. This is based on the X-ray structure for Cu^{II}(P-3A), a biosynthetic precursor of BLM, which has four in-plane donors of imidazole, deprotonated amide, pyrimidine and secondary amine. An axial terminal amine of β-aminoalanine completes the coordination [2]. The extent of involvement of the amide moiety, a nearby mannose and the β-aminoalanine moiety at the BLM site has been disputed by several workers [2, 3]. The extent of coordination of these groups may be different depending on the metal ion present. In particular, the amide anion is not likely to be favored by Cu^{I}. Since Fe^{II} readily displaces Cu^{I} from Cu^{I}(BLM), it is assumed that the Fe^{II}(BLM) complex is most important as the active metal complex [2]. The Fe^{II}(BLM) complex exhibits a pK_a of 5.6, suitable for formation of the Fe^{II}–amide anion bond under physiological conditions; thus the N_5 donor set found for Cu^{II}(P-3A) has been assumed for the Fe^{II}BLM complex which binds O_2.

There is much current interest in the structures of metal complexes related to the metallo-binding core of Fe^{II}(BLM) or Cu^{II}(P-3A) in order to understand the reactivity of BLMs. The active iron–oxygen derivative is best described as a ferryl $Fe^{III}O$(BLM)

0020-1693/90/$3.50

complex [7–14]**. The Fe(BLM) complex binds along the minor groove of DNA, making contacts with metal binding region, the bithiazole unit and cationic terminus. The latter two units provide the high association constant of *c.* 10^5 M^{-1} for binding of Fe^{II}(BLM) to the DNA substrate. The metal ion binding region is placed near the hydrogen of the C-4 position of the deoxyribose. It is postulated that the ferryl $Fe^{III}O$(BLM) abstracts the C-4H. The resultant radical adds O_2 which is reduced to a reactive hydroperoxide. Further decomposition of the hydroperoxide leads to dissociation of a base propenal of the DNA base at the site of scission; details have been given in the reviews of Hecht [3a] and of Stubbe *et al.* [3b, 13]. A pathway resultant from cross-coupling of a coordinated hydroxyl and C-centered radical leads to hydroxylation at C-4. This route produces loss of the free DNA base upon hydrolysis of the hydroxylated deoxyribose [3]. Free HO· may be generated in homogeneous solution by an alternate reductive pathway [7–14].

DNA cleavage patterns of BLMs, which show preferential breaks at GC(5′ → 3′) and GT(5′ → 3′) sequences, are significantly different from the $Fe^{II}(edta)^{2-}$-based (Dervan-type) cleavage complexes utilizing free HO· [15, 16]. Modifications in the BLM activity produced by changes in the bithiazole, cationic terminus or sugar moieties have been studied previously [2b, c; 3–6]. Cleavage specificity, together with minor groove binding, is influenced by the structure of the metal ion binding region [17, 3]. Chemical modifications of the donor units in the metal binding region might change the cleavage specificity, enhance activity or produce antitumor activity against BLM-resistant tumors. An understanding of the structural features of the metal ion binding core which are necessary for reactivity is clearly desirable.

Models of the metal binding region include Cu(PMA)$^+$ [18, 19], and M(PYML)†, M(AMPHIS) [27, 31]†, M(HAPH) [28, 29]†, and M(SAPH-3) [28, 30]† (M = Fe^{II} or Cu^{II}). Structural data from X-ray crystallographic studies have been previously limited to the Cu(PMA)$^+$ complex [18] and Cu^{II}(P-3A) [2]. Both structures are distorted square pyramids which include a coordinated, deprotonated in-plane amide donor [18, 32]. Detailed solution studies of the Fe^{II} and Cu^{II} complexes or PYML, AMPHIS, HAPH and SAPH-3 have been carried out in several laboratories. Identification of the species and other pH-dependent forms has involved a variety of spectral, magnetic resonance and electrochemical techniques [18, 27–30]. Similar chemical behavior of the complexes of these BLM models has been observed. The Fe^{II} derivatives exhibit equilibrium (1) in the pH range of 6 to 9, shifting to the right with increasing pH [31]††. The structure with five donors is consistent with most favored binding requirements for O_2 as found for polyamine and porphyrin Fe^{II} and Co^{II} complexes [20–26].

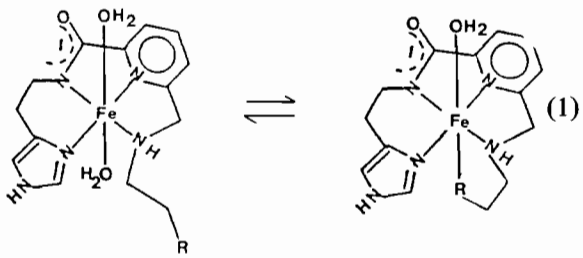

	AMPHIS, PYML	HAPH	SAPH-1	SAPH-3
R	$-NH_2$		$-SCH_3$	$-SH$

In this report we provide X-ray structural data for the [Cu(HAPH)]$(ClO_4)\cdot 1.6H_2O$ complex. The Cu^{II} center is bound in a distorted square pyramid. This structure is compared to the [Cu(PMA)]ClO_4 salt of Mascharak [18]. Additional reactivity studies have been carried out using the Fe^{II} complexes of HAPH, AMPHIS and SAPH-3. The ability of Fe^{II} derivatives of BLM core model ligands to activate O_2 and to cleave plasmid pT181 supercoiled DNA and a 450 base-pair TaqI restriction fragment of pT181 has been evaluated with authentic BLM serving as a control.

BLM core model complexes used in this study include HAPH, AMPHIS and SAPH-3:

**It should be noted, however, that Umezawa *et al.* have observed evidence for two reactive forms of activated Fe(BLM) [11, 2]. Although the work of Hecht *et al.* has shown 'active FeBLM' carries out O atom transfer to olefins [12], typical of the reactions of metal oxo (ferryl) complexes, the observed release of DNA bases from the C-1 sugar position by one oxidative cleavage pathway is consistent with coordinated hydroxyl activity which can be induced from one resonance of an Fe^{III}–O-atom complex [13, 14].

†Preferred donors include an N_5 donor set [20, 21], an in-plane amide group [22, 23], and a π-donating axial base such as imidazole or thiolato sulfur [24–26]. Both Fe^{II} complexes capable of generating 'active oxygen' or HO· and their redox inactive Cu^{II} complexes have been characterized for PYML, AMPHIS, HAPH and SAPH-3 [27–30]. Ligands related to AMPHIS have also been prepared with Fe^{II} and Cu^{II} derivatives [31].

††The Cu(PMA)$^+$ structure [18] is in keeping with axially coordinated R moieties (equilibrium (1)) and a remaining labile solvent position available for O_2 binding in the Fe^{II} derivatives.

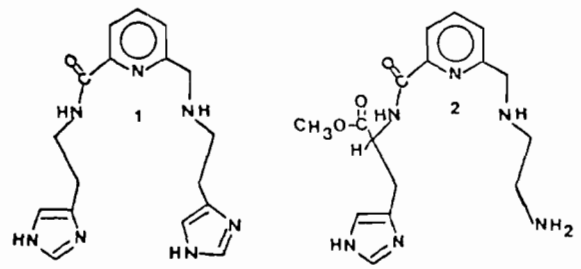

1 = HAPH

2 = AMPHIS

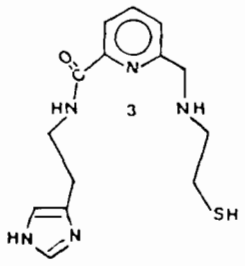

3 = SAPH-3

Experimental

Ligands

The ligands HAPH and SAPH-3 were prepared by published procedures [28–30]. AMPHIS was a kind gift of J.-P. Henichart. Blenoxane was a gift of Bristol-Meyers Company.

[Cu(HAPH)](ClO$_4$)·1.61H$_2$O

The crystal used in the X-ray diffraction was obtained by allowing 1 mmol of Cu(CH$_3$CO$_2$)$_2$·H$_2$O to react with 1.2 mmol HAPH in 40 ml of CH$_3$OH. Three equivalents of LiClO$_4$ were added. The deep blue solution was filtered through glass wool and the solution was allowed to evaporate at room temperature. Dark blue–green blocks were isolated by filtration after 48 h. A suitable crystal was mounted for X-ray analysis as described below.

Instrumentation

The ligands HAPH and SAPH-3 were chromatographed and analyzed for purity using a JEOL-FX90Q ^{1}H NMR spectrometer. Details were reported elsewhere [27–30]. An infrared spectrum of [Cu(HAPH)](ClO$_4$)·1.61H$_2$O was obtained in a KBr pellet pressed at 10 tons. A FT-IR spectrum was obtained on a Perkin-Elmer Model 32 FT-IR. X-ray diffraction data was collected on a Rigaku AFC5 diffractometer equipped with a rotating anode source. Cu Kα radiation of 1.540598 Å was used.

Crystal Structure Parameters

The following cell parameter data was obtained. [C$_{17}$H$_{20}$ON$_7$Cu](ClO$_4$)·1.607H$_2$O, M_r = 501.39, monoclinic, $C2/c$, a = 25.6516(21), b = 8.0487(7), c = 23.7624(17) Å, β = 118.114(5)°, V = 4326.71(65) Å^3, Z = 8, D_x = 1.5393 Mg m^{-3}, μ = 2.986 mm^{-1}, $F(000)$ = 2184.5352, T = 296 K, R = 0.064 for 2897 unique observed reflections.

X-ray Diffraction Data Collection

A bright blue plate-like crystal [Cu(HAPH)](ClO$_4$)·1.61H$_2$O of dimensions 0.2 × 0.2 × 0.1 mm was used to obtain cell parameters and collect diffraction intensity data. Using a 'search' routine 20 reflections were chosen to obtain an initial matrix. Cell dimensions were then obtained using a least-squares refinement procedure on 20 high angle reflections. Data were collected at 16°/min with $2\theta-\omega$ scans performed. 50% of the time was spent on background measurement. Three standard reflections were used to monitor decay and crystal orientation. The standards showed no decrease in intensity during the course of data collection. Data was collected to a 2 max of 120, with an index range of $0 \leqslant h \leqslant 29$, $0 \leqslant k \leqslant 9$, $-27 \leqslant l \leqslant 27$. Psi scans were conducted on three reflections to account for absorption due to crystal morphology. A total of 3557 diffraction intensities was measured of which 2543 were considered observed with a 10 σF cut-off on the pre-scan. Absorption, decay and Lorentz polarization corrections were applied using a Rigaku supplied program TXTMSC. The crystal structure was solved and refined using a direct method program SHELX from fifty E values greater than 1.2 and refined using UPALS [33]. Difference Fouriers were calculated to locate H atoms. 16 H atoms were located and successfully refined with isotropic temperature factors. H5 and H16 were placed in idealized positions and not refined. Two water molecules were located on the difference maps and the O atoms were anisotropically refined. One of them had a partial occupancy of 60.67%. Only one water H was located and isotropically refined. The perchlorate counterion was located and anisotropically refined. The function minimized in the refinement was $[w(k|F_o| - |F_c|)^2]$ with $w = 1/\sigma^2(|F_o|)$, where $\sigma(|F_o|) = [2(|F_o|^2) + (0.02F_o^2)]^{1/2}/(2|F_o^2|)$ and $\sigma(F_o^2)$ was obtained from counting statistics. The structure was refined to an $R(F)$ = 0.064 $R_w(F)$ = 0.095 for 2897 of the 3536 measured reflections and 363 refined parameters. The maximum parameter shift/e.s.d. ratio in the final least-squares cycle was 0.021. A final difference Fourier synthesis showed no significant residual density with ρ_{max} = 0.170 and ρ_{min} = −0.660 and mean residual electron density = 0.04 e$^-$/Å^3.

DNA Cleavage Studies

Plasmid pT181 DNA, used throughout this work, was isolated from *Staphylococcus aureus* and has been completely sequenced [34]. Restriction and modifying enzymes were purchased from Bethesda

Research Labs. (Gaithersburgh, MD), and used according to the manufacture's directions. [^{32}P] labeled ATP was obtained from ICN (California).

Weighed samples of the ligands were prepared and dissolved in 50 mM Tris pH 8 to achieve a final concentration of 0.40 mM. Solid $Fe(NH_4)_2(SO_4)_2 \cdot 6H_2O$ was added such that the Fe^{II} concentration was 0.10 mM. Chelation was allowed to proceed for 1 min after which time the Fe^{II}–ligand complex was added to the DNA. In the case of the $Fe^{II}(edta)^{2-}$, the initial concentration of edta was 40 mM and the complex was 20 mM. Supercoiled plasmid pT181 (1 μg) was incubated with various concentrations of the Fe^{II}–ligand complexes as described in the Figure legends. The DNA cleavage reactions were carried out in 15 μl volumes of a buffer consisting of 50 mM Tris–HCl pH 8.0 and 1 mM dithiothreitol. Reactions were allowed to proceed for 5 min at room temperature and, then, were quenched by the addition of 1 μg of tRNA. The samples were adjusted to 20 mM Na_2H_2edta and 5% glycerol and quickly loaded onto a 1% agarose gel. After electrophoresis at 10 V/cm for 3 h, the gel was stained with ethidium bromide and photographed under ultraviolet illumination.

A 650 base pair TaqI fragment of pT181 was isolated from a polyacrylamide gel and 5'-end-labeled with ^{32}P by standard procedures [35]. This fragment was recut with MboI and a 450 base pair fragment (which was labeled at a single end) was isolated. This fragment was reacted with the Fe^{II}–ligand complexes in the presence of O_2 and dithiothreitol as described above except that 10 ng (approximately 2×10^5 cpm) of labeled DNA was mixed with 1 μg of sonicated salmon sperm DNA. The reaction volume was 100 μl. The reactions were quenched by adding 10 μg tRNA and 0.1 volume of 3 M sodium acetate. The DNA was precipitated twice with ethanol. The dried DNA pellets were resuspended in 6 μl of 50% formamide containing bromphenol blue and xylene cyanol and loaded onto an 8% polyacrylamide–urea sequencing gel. The labeled fragment was also subjected to the A + G and C + T Maxam and Gilbert sequencing reactions [36], which served as gel markers. Electrophoresis was carried out at 1200 V for 5 h and the gel was exposed to X-ray film at −70 °C for 5 days.

Results and Discussion

[Cu(HAPH)](ClO$_4$)·1.61H$_2$O Complex

The infrared (FT-IR) spectrum of $[Cu(HAPH)](ClO_4) \cdot 1.61H_2O$ is shown in Fig. 1. An intense carbonyl-amide band is observed at 1574 cm^{-1} indicative of a deprotonated amido N coordinated to Cu^{II} [37]. The corresponding band for $[Cu(PMA)](ClO_4)$ is at 1600 cm^{-1} [18]. Related Cu^{II} complexes which have coordinated amide groups within ligand

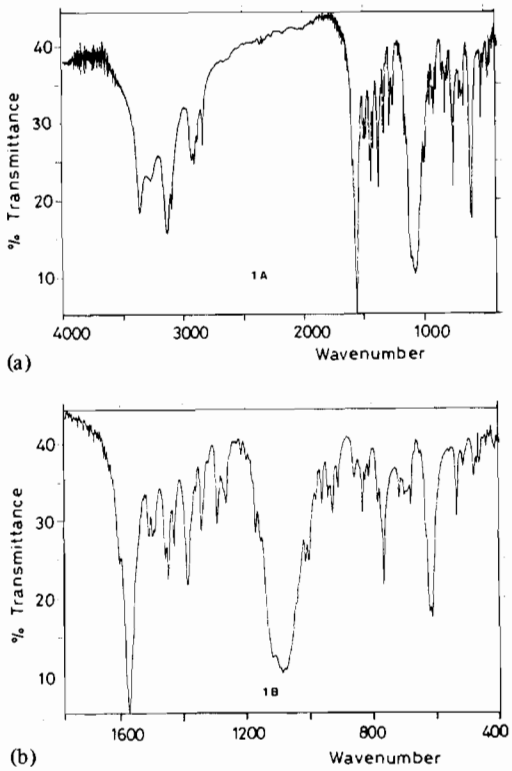

Fig. 1. FT-IR spectrum of $[Cu(HAPH)](ClO_4) \cdot 1.6H_2O$ in KBr: (a) 4000–400 cm^{-1}; (b) 1800–400 cm^{-1}; expanded scale.

structures which model fragments of the in-plane BLM donor set are $[Cu(Pypep)(CH_3CO_2)_2] \cdot 1.46H_2O$ and $Cu(Pmpep)(CH_3CO_2)$ [38]. These salts exhibit amide carbonyl bands at 1585 and 1620 cm^{-1}, respectively compared to 1650 and 1665 cm^{-1} for the free ligands [38]. The coordinated amide is confirmed by the X-ray structural data given below.

An ORTEP drawing [39] of the $Cu(HAPH)^+$ cation is shown in Fig. 2. The coordination geometry is seen to be a distorted square pyramid with the terminal imidazole (N22) serving as the axial donor. In-plane donation from the pyridine (N1), amine (N18), amido (N9) and imidazole (N13) donors are obtained. Positional parameters and isotropic temperature factors for the non-hydrogen atoms are given in Table 1. Bond distances and selected angles are given in Tables 2 and 3, respectively. See also 'Supplementary Material'. Least-squares planes show that the Cu^{II} center is 0.062 Å above the plane defined by the four 'in-plane' N donors and displaced toward the axial donor N22; imidazole nitrogen N13 is displaced 1.03 Å below the plane. An alternate description of the complex as a severely distorted trigonal bipyramid might be given. However, the similarity to the $Cu(PMA)^+$ structure is shown by the comparison data in Table 4 which expresses the equivalent Cu^{II}-donor positions according to the numbering scheme of

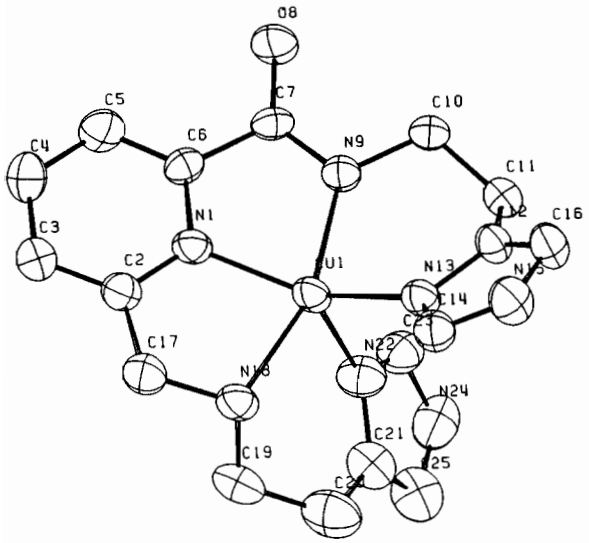

Fig. 2. ORTEP diagram of $[Cu(HAPH)]^+$; ellipsoids represent 50% probabilities.

TABLE 1. Positional parameters of non-hydrogen atoms and their isotropic temperature factors

	x	y	z	B_{eq}
Cu1	0.3189(0)	0.5891(1)	0.4297(0)	3.16(3)
N1	0.2434(2)	0.6834(5)	0.4150(2)	2.41(15)
C2	0.1960(3)	0.5897(7)	0.3954(3)	2.71(19)
C3	0.1413(3)	0.6600(8)	0.3812(3)	3.18(21)
C4	0.1393(3)	0.8296(8)	0.3895(3)	3.41(21)
C5	0.1902(3)	0.9229(7)	0.4124(3)	3.20(24)
C6	0.2422(2)	0.8488(7)	0.4244(3)	2.36(17)
C7	0.3022(3)	0.9254(6)	0.4532(3)	2.53(19)
O8	0.3088(2)	1.0756(4)	0.4715(2)	3.30(15)
N9	0.3450(2)	0.8233(5)	0.4590(2)	2.43(15)
C10	0.4049(3)	0.8842(8)	0.4934(3)	3.04(22)
C11	0.4498(3)	0.7560(8)	0.4958(3)	2.93(20)
C12	0.4462(3)	0.5937(7)	0.5238(3)	2.60(19)
N13	0.3954(2)	0.4941(6)	0.4955(2)	2.44(15)
C14	0.4074(3)	0.3545(7)	0.5304(3)	2.79(19)
N15	0.4630(2)	0.3616(7)	0.5783(3)	3.45(19)
C16	0.4886(2)	0.5097(8)	0.5749(3)	3.15(20)
C17	0.2087(3)	0.4081(9)	0.3981(5)	3.53(27)
N18	0.2655(2)	0.3725(6)	0.3983(2)	2.88(16)
C19	0.2567(3)	0.3059(9)	0.3349(3)	4.21(25)
C20	0.3115(4)	0.2780(9)	0.3324(4)	4.72(31)
C21	0.3352(3)	0.4320(8)	0.3189(3)	3.62(22)
N22	0.3355(2)	0.5799(6)	0.3484(2)	3.02(17)
C23	0.3579(3)	0.6920(9)	0.3257(3)	3.58(22)
N24	0.3721(2)	0.6270(8)	0.2830(3)	4.13(21)
C25	0.3574(4)	0.4628(12)	0.2786(4)	4.66(30)
Cl1	0.4567(4)	1.0368(2)	0.3213(1)	3.44(6)
O1	0.4474(1)	1.0200(2)	0.3755(1)	8.59(33)
O2	0.4033(3)	1.0202(11)	0.2660(3)	7.45(26)
O3	0.4849(3)	1.1909(9)	0.3274(3)	7.65(31)
O4	0.4947(3)	0.9070(7)	0.3259(3)	8.33(35)
OW1	0.8030(2)	0.1944(7)	0.3026(3)	4.89(21)
OW2	0.5013(27)	0.4214(11)	0.2544(20)	6.76(68)

TABLE 2. Bond distances for the $[Cu(HAPH)]^+$ cation

Atoms	d (Å)	Atoms	d (Å)
Cu–N1	1.952(5)	C16–C12	1.368(9)
Cu–N9	2.013(5)	C17–N18	1.482(10)
Cu–N13	1.998(5)	C19–N18	1.496(9)
Cu–N18	2.124(5)	C19–C20	1.504(12)
Cu–N22	2.168(6)	C20–C21	1.482(11)
C2–N1	1.316(8)	C21–C25	1.348(12)
C6–N1	1.353(8)	C21–N22	1.380(9)
C2–C3	1.398(9)	C23–N22	1.315(9)
C17–C2	1.492(10)	C23–N24	1.336(10)
C4–C3	1.384(10)	C25–N24	1.365(12)
C5–C4	1.377(10)		
C5–C6	1.363(10)		
C6–C7	1.494(8)		
C7–O8	1.269(8)		
C7–N9	1.326(8)		
C10–N9	1.443(9)		
C10–C11	1.528(10)		
C11–C12	1.490(9)		
C12–N13	1.403(8)		
C14–N13	1.344(8)		
C14–N15	1.341(9)		
C16–N15	1.382(9)		

TABLE 3. Bond angles of the $[Cu(HAPH)]^+$ cation

Bond angle	Degrees	Bond angle	Degrees
N9–Cu–N1	80.7(2)	C10–N9–Cu	127.4(4)
N13–Cu–N1	144.6(2)	C10–N9–C7	117.2(5)
N13–Cu–N9	92.5(2)	C11–C10–N9	112.0(6)
N18–Cu–N1	80.5(2)	C12–C11–C10	110.2(5)
N18–Cu–N9	161.0(2)	N13–C12–C11	121.8(5)
N22–Cu–N1	116.7(2)	C16–C12–C11	129.7(6)
N18–Cu–N13	101.2(2)	C16–C12–N13	108.3(5)
N22–Cu–N13	98.7(2)	C12–N13–Cu	120.4(4)
N22–Cu–N9	99.6(2)	C12–N13–C14	106.9(5)
N22–Cu–N18	91.4(2)	N15–C14–N13	109.3(5)
C2–N1–Cu	120.9(4)	C16–N15–C14	109.4(6)
C6–N1–Cu	116.9(4)	N15–C16–C12	106.0(6)
C6–N1–C2	122.2(5)	N18–C17–C2	112.6(7)
C3–C2–N1	120.6(6)	C14–N13–C12	106.9(5)
C17–C2–N1	113.6(6)	C19–N18–Cu	115.5(4)
C17–C2–C3	125.5(6)	C19–N18–C17	110.6(6)
C4–C3–C2	117.8(6)	C20–C19–N18	111.8(6)
C5–C4–C3	120.1(6)	N22–C21–C20	121.0(7)
C6–C5–C4	119.8(6)	C25–C21–C20	131.5(8)
C5–C6–N1	119.6(6)	C25–C21–N22	107.5(7)
C7–C6–N1	112.5(5)	C21–N22–Cu	121.8(4)
C7–C6–C5	127.8(6)	C23–N22–Cu	130.5(5)
C6–C7–O8	119.4(5)	C23–N22–C21	106.4(6)
N9–C7–C6	114.7(5)	N24–C23–N22	111.8(6)
N9–C7–O8	125.9(6)	C25–N24–C23	105.9(7)
		N24–C25–C21	108.5(8)

TABLE 4. Structure comparison of $Cu(PMA)^+$ and $Cu(HAPH)^+$

	$Cu(PMA)^+$				$Cu(HAPH)^+$		
Bonds							
Cu–N1(in	2.10(3)[a]		1.93(1)[b]		1.998(5)		(Cu–N13)
Cu–N3(ar	1.86(2)		1.97(1)		2.013(5)		(Cu–N9)
Cu–N5(p)	2.17(2)		1.97(1)		(py)1.952(5)		(Cu–N1)
Cu–N6(ar	2.18(2)		2.13(1)		2.124(5)		(Cu–N18)
Cu–N7(a)	2.19(2)		2.23(1)		(imz)2.168(6)		(Cu–N22)
Average	2.10(3)		2.05(1)		2.051(6)		
		Δ[c]		Δ[c]		Δ[c]	
In-plane angles							
N1–Cu–N3	82.7	7.3	95.4(4)	5.4	92.5(2)	2.5	(N1–Cu–N9)
N3–Cu–N5	91.6	1.6	79.4(4)	10.6	80.7(2)	9.3	(N9–Cu–N13)
N5–Cu–N6	65.7	24.3	79.9(4)	10.1	80.5(2)	9.5	(N1–Cu–N18)
N1–Cu–N6	117.5	27.5	102.8(4)	12.8	101.2(2)	11.2	(N18–Cu–N13)
	sum = 357.5	ave. = 15.2	sum = 357.5	ave. = 9.7	sum = 354.9	ave. = 8.1	
Axial angles							
N1–Cu–N7	96.3	6.3	99.7(4)	9.7	98.7(2)	8.7	(N22–Cu–N13)
N6–Cu–N7	83.8	6.2	83.5(4)	6.5	91.4(2)	1.4	(N22–Cu–N18)
N5–Cu–N7	103.3	13.3	101.7(4)	11.7	116.7(2)	26.7	(N22–Cu–N1)
N3–Cu–N7	105.8	15.8	103.6(4)	13.6	99.6(2)	9.6	(N22–Cu–N9)
	sum = 389.2	ave. = 10.4	sum = 388.5	ave. = 10.4	sum = 406.4	ave. = 11.6	

[a] BF_4^- salt, ref. 18. [b] ClO_4^- salt, ref. 19. [c] $\Delta = |(90° - \angle)|$.

Mascharak *et al.* [18, 19] for the $Cu(PMA)^+$ complex. Data for the BF_4^- salt of $Cu(PMA)^+$ [18] was reported, followed by a more complete report of a ClO_4^- salt [19] by Mascharak *et al.* The average Cu–N bond distances and angles are similar between $Cu(PMA)^+$ and $Cu(HAPH)^+$. The major differences are noted as follows: $Cu(PMA)^+$ has a 0.15 Å shorter Cu^{II}–amide bond for the BF_4^- case; this is reduced to 0.043 Å when ClO_4^- salts are compared. A 0.22 Å shorter Cu^{II}–pyridine versus Cu^{II}–pyrimidine bond in $Cu(HAPH)^+$ versus $Cu(PMA)^+$ is consistent with the more basic pyridine for HAPH versus pyrimidine for PMA in the BF_4^- salt; the distances are nearly the same in the ClO_4^- comparison. The 'in-plane' angles are closer to the theoretical 90.0° for a square pyramid in $Cu(HAPH)^+$. The average deviation from 90.0° is 8.1° for $Cu(HAPH)^+$ versus 15.2° (BF_4^-) or 9.7 °C (ClO_4^-) for $Cu(PMA)^+$. The deviation from 90.0° axial angles is only slightly smaller for $Cu(PMA)^+$; 10.4° for $Cu(PMA)^+$ versus 11.6° for $Cu(HAPH)^+$. $Cu(PMA)^+$ has been described as a distorted square pyramid [18, 19]; therefore, it appears justified to describe $Cu(HAPH)^+$ as a distorted square pyramid. See 'Supplementary Material' for complete data.

The influence of the metal center on any perturbation of the imidazole rings is of interest. The angles in both imidazole rings of $Cu(HAPH)^+$ average the expected 108°. The N22–C21 distance (1.380 Å) of the axial imidazole donor is significantly shorter than the N13–C12 distance (1.403 Å) of the 'in-plane' imidazole. All other distances in these rings are correspondingly very close to each other (Table 5). A comparison with the average distances which are found in literature values of the distances for 1-methylimidazole complexes Mg^{II}, Mn^{II}, Fe^{II} and Co^{II} porphyrins [41] is also provided in Table 5. The N22–C21 and N13–C12 bonds correspond to the N3–C4 bond in the standard numbering scheme for imidazole rings, e.g. N_3 as the coordinated nitrogen atom, N_1 as the pyrrole nitrogen and C_4 as the near carbon. The same bond is observed to be 1.42(2) Å in the $Cu(PMA)^+$ complex as in the ClO_4^- salt [19]. The normal length for coordinated 1-methyl-

TABLE 5. Comparison of coordinated imidazole rings of $[Cu(HAPH)]^+$ and $[Cu(PMA)]^+$

	Ring				
	N_3-C_2	N_3-C_4	C_4-C_5	C_5-N_1	N_1-C_2
Axial imz > $[Cu(HAPH)]^+$	1.315(9)	1.380(9)	1.348(12)	1.365(12)	1.336(10)
In-plane imz > $[Cu(HAPH)]^+$	1.344(8)	1.403(8)	1.368(9)	1.382(9)	1.341(9)
In-plane-$[Cu(PMA)]^+$ [19]	1.31(2)	1.42(2)	1.36(2)	1.36(2)	1.36(2)
$[(NH_3)_5Co(5CH_3\text{-imz})]^{3+}$ [40]	1.311(8)	1.410(7)	1.371(8)	1.371(8)	1.344(7)
Average 1-CH_3im (lit.)[a]	1.308	1.375	1.346	1.351	1.340
imz [42]	1.326	1.378	1.358	1.369	1.349

[a]Literature average from $Mg(H_2O)_2(CH_3im)_2^{2+}$, Mg(TPP)(1-$CH_3$im)$_2$, Mn(TPP)(1-$CH_3$im), Fe(TPP)NO(1-$CH_3$im) and Co(TPP)(1-$CH_3$im); ref. 41.

imidazoles is 1.375 Å for the N_3-C_4 bond [41]; this length is virtually the same as observed for imidazole itself (1.378 Å) [42] in which imidazole units are H-bonded in a staggered arrangement. The axial imidazole ring is therefore unperturbed in the N_3-C_4 bond, while the in-plane imidazoles in both Cu(HAPH)$^+$ and Cu(PMA)$^+$ are elongated *c.* 0.025 and 0.042 Å, respectively. The same influence on the N_3-C_4 bond has been observed with the 5-methylimidazole complex of pentaamminecobalt(III), $(NH_3)_5Co(5CH_3\text{-imz}^{3+})$ [40]. In the Co(III) complex, Co(III) is known to perturb the hybridization at the C_2 and C_4 carbons [42, 43]. This results in downfield shifts for the protons at C_2 and C_4 which have been shown via its Rh(III) analog [43] to be due predominantly by a rehybridization influence rather than temperature independent paramagnetism. Therefore, the influence of Co(III) appears to be due to the σ-withdrawing influence from a metal center of relatively high effective nuclear charge. One notes from prior studies of M(II) complexes with porphyrins [41] where the metal center has a metal of much lower effective charge, that the N_3-C_4 bonds remain almost the same as in free imidazole (1.375 versus 1.378 Å) [41]. The interesting conclusion is that Cu(II) which has the largest effective nuclear charge of any 2+ ion of the first transition series acts as a strong σ-withdrawing metal center toward the in-plane imidazole ring in both Cu(HAPH)$^+$ and Cu(PMA)$^+$, but its influence is much less toward the axial imidazole of Cu(HAPH)$^+$. This latter observation is manifest due to the 0.17 Å longer bond to the axial imidazole in Cu(HAPH)$^+$, indicative of a weaker σ-donation toward Cu(II) by the axial ligand.

With Cu^{II} no special effects due to π-backbonding from Cu^{II} or π-donation from the imidazoles is anticipated. However, the influence of the metal ion–imidazole interaction is probably quite important for the Fe^{II} and Fe^{III} derivatives. The bond distances in the amide region show an elongation of the C7–O8 bond (1.269 Å, $\Delta = +0.054$ Å) relative a normal keto carbonyl (*c.* 1.215 Å), a shortening of the C7–N9 bond (1.326 Å, $\Delta = -0.146$ Å) relative to the typical C–N single bond of 1.472 Å, and a slightly shorter C6–C7 bond (1.494 Å, $\Delta = -0.043$ Å) compared to the typical C–C single bonds. The distances observed for the amide are typical of peptides [44]: d(C–O) ~ 1.24 Å, d(C–N) ~ 1.32 Å. The angles about C7 are also similar to peptides [44]: C6–C7–O8, 119.4(5)° (121°); O8–C7–N9, 125.9(6)°(125°); C6–C7–N9, 114.7(2)°(114°).

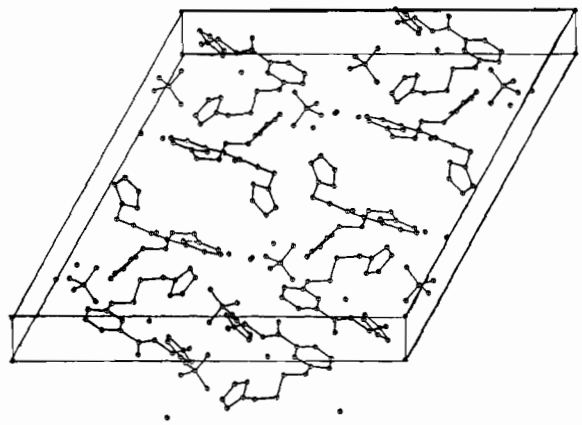

Fig. 3. Molecular packing diagram of $[Cu(HAPH)](ClO_4)\cdot 1.607H_2O$.

The molecular packing diagram for $[Cu(HAPH)](ClO_4)\cdot 1.61H_2O$ is shown in Fig. 3. The tilt of the 'in-plane' imidazole donor (N13) out of the best square plane and the additional tilt of the axial imidazole (N22) away from 90.0° is clearly observable. The presence of the ClO_4^- ion near the pyrrole NH of the axial imidazole is also observed, but the distance of greater than 2.4 Å rejects H-bonding between them. The distance between the pyrrole NH of the 'in-plane' imidazole and the nearby ClO_4^- (N15–O1) is 1.846(10) Å. This is clearly a good H bond for this pair. However, the (N15–O4) distance is also 2.060(10) which is within an H-bonded distance. The ClO_4^- ion distances and angles are normal: 1.423(8), 1.388(7), 1.409(8), 1.398(8) Å; 109.7(5),

105.1(4), 106.7(5), 105.5(5), 114.6(3), 110.1(5)° (ave. = 109.6°). A herringbone packing pattern shows the C25H of the axial imidazole ring pointed toward the pyridine aromatic ring similar to the fashion of the benzene crystal structure. The additional tilt of the axial imidazole (N22) is probably due in part to the six-membered axial ring in the $Cu(HAPH)^+$ cation compared to a five-membered axial ring in $Cu(PMA)^+$. A curious difference between $Cu(HAPH)^+$ and $Cu(PMA)^+$ is that the axial donors are on opposite sides of the plane defined by the in-plane donors. One reason for preferring to describe the $Cu(HAPH)^+$ complex as a distorted square pyramid rather than a distorted trigonal bipyramid comes from the ESR spectrum of the complex. The $Cu(HAPH)^+$ ESR spectrum is that of a tetragonal Cu^{II} site rather than a trigonal bipyramidal site. The latter would produce a reversed ESR pattern which is not observed in a 50:50 DMSO:water glass at 77 K. Rather an axial type spectrum with $g_{\parallel} = 2.22$, $g_{\perp} = 2.06$, $A_{\parallel} = 201 \times 10^{-4}$ cm^{-1} has been reported [29]. These parameters are quite close to the values for Cu(BLM): $g_{\parallel} = 2.19$, $g_{\perp} = 2.04$, $A_{\parallel} = 189 \times 10^{-4}$ cm^{-1}; or $Cu(PMA)^+$: $g_{\parallel} = 2.21$, $g_{\perp} = 2.05$, $A_{\parallel} = 190 \times 10^{-4}$ cm^{-1} [18] (184×10^{-4} cm^{-1}) [19].

DNA Cleavage by BLM Models

Based on the similarity of the visible spectral properties of $Fe^{II}(BLM)$ and $Fe^{II}(HAPH)$ and the electrochemical behavior for them, as well as Kimura's L_2 complex, $Fe^{II}(HAPH)$ appears to have the N_5 coordination of $Fe^{II}(BLM)$; e.g. the solvated structure of $Cu^{II}(HAPH)^+$ [29, 31]. Since the pyrrole NH of imidazole and imidazolium rings are known to make strong H bonds to phosphates, it was deemed an interesting study to see if $Fe^{II}(HAPH)$ is active in DNA cleavage activity and if the presence of a second imidazole produces a significant change in DNA cleavage relative to $Fe^{II}(BLM)$ and other BLM core models.

The ability of the Fe^{II} derivatives to cleave plasmid pT181 supercoiled DNA or its 650 base pair TaqI restriction fragment has been examined in comparison with $Fe^{II}(BLM)$ and $Fe(edta)^{2-}$ *in vitro* to assess the influence of the axial imidazole donor in $Fe^{II}(HAPH)$. The observed DNA-cleavage activity parallels the HO· generating capacity from O_2 [27–30, 45]*: $Fe^{II}(BLM) > Fe^{II}(HAPH) > Fe^{II}(AMPHIS) > Fe^{II}(SAPH\text{-}3) \cong Fe^{II}(edta)^{2-}$ ($1 \times 10^4 : 2 \times 10^3 : 5 \times 10^2 : 1 : 1$). An analysis of the ability of bleomycin metal binding core analogs to cleave supercoiled plasmid DNA is shown in Fig. 4. The position of the supercoiled (form I), nicked open-circular (form II), and linear (form III) plasmid DNA is indicated. By

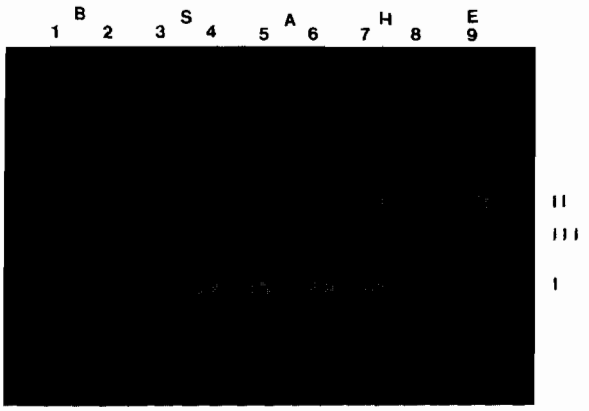

Fig. 4. Cleavage of supercoiled DNA by the metal binding core analogs. Supercoiled plasmid pT181 was incubated with the metal binding core analogs as described in ref. 37. Lane 1 contains plasmid DNA alone; lane 2 contains plasmid DNA incubated with 40 μM HAPH without added iron; lanes 3 and 4 contain DNA incubated with 20 and 40 μM Fe^{II}(SAPH-3) respectively; lanes 5 and 6 contain DNA incubated with 20 and 40 μM Fe^{II}(AMPHIS) respectively; lanes 7 and 8 contain DNA incubated with 20 and 40 μM Fe^{II}(HAPH); lane 9 contains DNA incubated with 4 mM $Fe^{II}(edta)^{2-}$. The various forms of the plasmid are indicated as follows: I = supercoiled plasmid; II = nicked (open) circular plasmid; III = linear plasmid.

comparison to the starting DNA it can be seen that the various analogs differ widely in their ability to cleave DNA. Fe^{II}(SAPH-3) had little or no effect on the plasmid at either 20 or 40 μM (lane 3 and 4), Fe^{II}(AMPHIS) showed a small amount of cleavage at 20 μM (lane 5). This activity appears as an increase in the amount of form II DNA and indicates that the lesions in the DNA are primarily single-strand nicks. At 40 μM Fe^{II}(AMPHIS) a small amount of linear plasmid DNA is found (lane 6) indicating the existence of either double strand cleavage or closely spaced single stranded nicks on opposite strands. In contrast, the amount of cleavage with 20 μM Fe^{II}(HAPH) (lane 7) is clearly more than that seen with 40 μM (AMPHIS). When the DNA is exposed to 40 μM Fe^{II}(HAPH) (lane 8), virtually all of the supercoiled DNA is converted to circular and linear forms. Furthermore, the linear DNA is cleaved to smaller fragments which appear as a smear in lane 8. As a control $Fe^{II}(edta)^{2-}$ was used at 4 mM (lane 9). $Fe^{II}(edta)^{2-}/O_2$ or H_2O_2 has previously been shown to cleave DNA [15, 16]. The activity of $Fe^{II}(edta)^{2-}$ is much lower than that of Fe^{II}(HAPH) (compare lanes 7 and 9).

A 450 base-pair singly end-labeled DNA fragment was prepared and incubated with the Fe^{II} complexes of the various core analogs. The results of this experiment are shown in Fig. 5. Controls consist of the fragment alone (lane 1) and the A + G and C + T chemical sequencing reactions [36] (lanes 2 and 3).

*DMPO: 5,5-dimethyl-1-pyrroline *N*-oxide; PBN: n-tert-butyl-α-phenylnitrone; for a review of the spin trapping technique see ref. 46.

Fig. 5. Cleavage of linear DNA by the metal binding core analogs. A 450 base pair DNA fragment labeled at one end with ^{32}P was incubated with the core analogs prior to electrophoresis on a polyacrylamide–urea sequencing gel followed by autoradiography. Lane 1 contains untreated DNA; lanes 2 and 3 contain DNA fragments generated by the A + G and C + T chemical sequencing reactions, respectively; lanes 4 and 5 contain DNA incubated with 20 and 40 μM Fe^{II}(HAPH), respectively; lanes 6 and 7 contain DNA incubated with 20 and 40 μM Fe^{II}(AMPHIS), respectively; lane 8 contains DNA incubated with 4 mM $Fe^{II}(edta)^{2-}$; lanes 9 and 10 contain DNA incubated with Fe^{II}(SAPH-3) at 20 and 40 μM, respectively.

The extent of cleavage by Fe^{II}(HAPH) (lanes 4 and 5), Fe^{II}(AMPHIS) (lanes 6 and 7), $Fe^{II}(edta)^{2-}$ (lane 8) and Fe^{II}(SAPH-3) (lanes 9 and 10) is consistent with the results of the cleavage of supercoiled DNA. An additional control lane with Fe^{II}(BLM) is not shown. Cleavage of DNA by $Fe^{II}(edta)^{2-}$ has been shown to be sequence independent [47]. This result is also seen in lane 8 where all of the cleavage fragments are present at approximately equal intensities. DNA cleavage by Fe^{II}(AMPHIS) also appears to show little, if any, sequence dependence. In contrast, Fe^{II}(HAPH) produces a variety of cleavage fragments of different intensities indicating possible sequence or structure-dependent cleavage. One consistent feature of Fe^{II}(HAPH) cleavage is an apparent lack of fragments which would result from cleavages at residues 3′ to a cytidine in the sequence of the fragment [34]. Fe^{II}(SAPH-3) shows a very slight ability to cleave linear DNA (lanes 9 and 10).

The efficacy of the bleomycins or drug metal chelates as antitumor drugs depends upon a number of factors: the ability to bind DNA, to activate oxygen and to produce DNA damage. Comparison with Fe^{II}(BLM) mediated DNA cleavage experiments indicates that Fe^{II}(HAPH) cleaves DNA-5 to ten-fold less efficiently than Fe^{II}(BLM) and 200-fold better than $Fe^{II}(edta)^{2-}$. Fe^{II}(HAPH) does, however, show less sequence specificity than bleomycin which has high affinity binding sites at G–T, G–C and G–A dinucleotide sequences [5].

Conclusions

Although the coordination geometry at the metal binding site of bleomycin remains a subject of debate, its overall nature appears to be important for specificity in DNA cleavage by $Fe^{II}(BLM)/O_2$ [3, 17]. Structural data have been limited to $Cu(PMA)^+$ and Cu(P-3A) [18, 32]. The additional structure of the $Cu(HAPH)^+$ complex shows the strong tendency of the Cu^{II} derivatives of BLM or its models to form square pyramidal complexes which are necessarily distorted by the irregular donor set. The structures of $Cu(HAPH)^+$, $Cu(PMA)^+$ and Cu(P-3A) and their frozen-glass ESR spectra show that there is some flexibility in the BLM core unit to adjust in the presence of differing axial donors to different bond lengths and angles without severe changes in the ESR parameters or UV–Vis spectra. The evidence for the coordination geometry for the Fe^{II} derivatives is even less certain due to the absence of any structure of Fe^{II}(BLM) or its models having been completed. However, the pH dependence of the UV–Vis spectra for complexes of HAPH, AMPHIS, BLM, SAPH-3 and Kimura's L_1 and L_2 ligands, as well as their electrochemical behavior, imply a similar solution structure for all of them [27–31]. The electrochemical behavior of Fe^{II}(BLM), Fe^{II}(HAPH), $Fe^{II}(L_1)$ and $Fe^{II}(L_2)$ [28–31] all support an N_5 donor set in support of a coordination site similar to the Cu^{II} complexes. An additional axial donor to complete the coordination number of six for the Fe^{II} derivatives is assumed.

If the in-plane donor set is held constant, the influence of the axial donor should prevail. The activity order of Fe^{II}(HAPH) (4X) > Fe^{II}(AMPHIS); (200X) > Fe^{II}(SAPH-3) or $Fe(edta)^{2-}$ is most probably due to differences in binding affinities since E° values for the nitrogen base donors in HAPH and AMPHIS show little difference. The surprising result is that about twenty percent of Fe^{II}(BLM) activity is obtained with Fe^{II}(HAPH) even though it lacks the side chain which assists minor groove binding in Fe^{II}(BLM). The reasons for an absence of cuts at positions 3′ to C remain unanswered by our limited set of data. However, it is tempting to note that C can

H-bond as the acceptor or H-donate to a unit along the minor groove while the other bases can only H-bond as the acceptor site. This might influence the most favored orientation of the in-plane amide relative to the DNA chain and deoxyribose units.

The results of the linear DNA and superhelical DNA cleavage studies indicate that manipulation of the metal binding core of bleomycin has dramatic effects on the ability to cleave DNA. The DNA cleavage results coupled with previous chemical analysis of oxygen activation by the metal binding core analogs [2] show that oxygen activation and DNA reactivity are interrelated as found for the whole Fe(BLM) system [10]. Synthesis of other analogs of the metal binding core which alter the chelation geometry, the donor groups which bind the metal, and oxygen activation ability will allow a direct correlation to be drawn between the essential structural features and the ability to cleave DNA. A series of synthetic molecules could also lead to an understanding of the structure–function relationships which lead to sequence-specific interaction with DNA. This presumably occurs via minor groove binding [17]. The physical size of the model systems are approximately 10 Å edge to edge and this size properly fits the minor groove, assisted by H-bonding forces.

Preliminary experiments show that Fe^{II}(HAPH) has the ability to inhibit the growth of mouse S180 sarcoma cells and to provide tumor cell kills with neuroblastoma cells*. It is possible that HAPH or a derivative of HAPH may have potential as an anti-tumor drug. It is further possible that this agent will kill cells which are resistant to the whole bleomycin molecule since a different transport mechanism may occur for species related to BLM but which lack the hydrophobic intercalator portion of the molecule.

Supplementary Material

Hydrogen atom fractional coordinates and e.s.d.s (Table SM-1; 1 page); anisotropic temperature factors for non-hydrogen atoms (SM-2; 2 pages); complete bond distance data and e.s.d.s (SM-3; 9 pages); complete bond angle data and e.s.d.s (SM-4; 57 pages); structure factors (F_{obs}, F_{calc}) for $[Cu(HAPH)]^+$ (SM-5; 18 pages) are available from the authors on request.

Acknowledgement

R.E.S. gratefully acknowledges support of the National Science Foundation Grant CHE8417751 for this work.

*Collaborative work in progress with Professor J. Lazo, Department of Pharmacology, University of Pittsburgh and Professor N. Shore, Children's Hospital, University of Pittsburgh.

References

1 H. Umezawa, K. Maeda, T. Takeuchi and Y. Okami, *J. Antibiot. (Tokyo), Sect. A, 19* (1966) 200.
2 (a) Y. Sugiura, T. Takita and H. Umezawa, Bleomycin antibiotics: metal complexes and their biological action, in *Metal Ions in Biological Systems,* Vol. 19, Marcel Dekker, New York, 1985, pp. 81–108; (b) M. Otsuka, M. Yoshida, S. Kobayashi, M. Ohno, Y. Sugiura, T. Takita and H. Umezawa, *J. Am. Chem. Soc., 103* (1981) 6986; (c) Y. Sugiura, *J. Am. Chem. Soc., 102* (1980) 5208.
3 (a) S. M. Hecht, *Acc. Chem. Res., 19* (1986) 383; (b) J. Stubbe and J. W. Kozarich, *Chem. Rev.,* (1987) 1107.
4 S. M. Hecht, in S. M. Hecht (ed.), *Bleomycin: Chemical, Biochemical and Biological Aspects,* Springer, New York, 1979.
5 H. Sugiyama, R. E. Kilkuskie, L.-H. Chang, L.-T. Ma, S. M. Hecht, G. A. van der Marcel and J. H. van Boom, *J. Am. Chem. Soc., 108* (1986) 3852.
6 Y. Sugiura, T. Suzuka, M. Otsuka, S. Kobayashi, M. Ohno, T. Takita and H. Umezawa, *J. Biol. Chem., 258* (1983) 1328.
7 Y. Sugiura, S. Ogawa and I. Morishima, *J. Am. Chem. Soc., 100* (1978) 3575.
8 R. M. Burger, S. B. Horowitz, J. Peisach and J. B. Wittenberg, *J. Biol. Chem., 254* (1979) 12299.
9 (a) R. E. White and M. J. Coon, *Ann. Rev. Biochem., 49* (1980) 315; (b) R. E. Kilkuskie, T. L. MacDonald and S. M. Hecht, *Biochemistry, 23* (1984) 6165.
10 R. M. Burger, J. Peisach and S. B. Horowitz, *J. Biol. Chem., 256* (1981) 11636.
11 H. Ekimoto, K. Takahashi, A. Matsuda, T. Takita and H. Umezawa, *Jpn. J. Antibiot., 38* (1985) 1077.
12 (a) D. C. Heinebrook, S. A. Carr, M. A. Mentzer, E. C. Long and S. M. Hecht, *Inorg. Chem., 26* (1987) 3835; (b) N. Murugesan and S. M. Hecht, *J. Am. Chem. Soc., 107* (1985) 493.
13 C. Wu, J. W. Kozarich and J. Stubbe, *J. Biol. Chem., 258* (1983) 4695.
14 R. M. Burger, J. Peisach and S. B. Horowitz, *J. Biol. Chem., 257* (1982) 8612.
15 (a) R. P. Hertzberg and P. B. Dervan, *J. Am. Chem. Soc., 104* (1982) 313; (b) P. B. Dervan, *Science, 232* (1986) 464; (c) P. G. Schultze, J. S. Taylor and P. B. Dervan, *J. Am. Chem. Soc., 104* (1982) 6861.
16 (a) J. H. Griffin and P. B. Dervan, *J. Am. Chem. Soc., 109* (1987) 6840; (b) J. P. Sluka, S. J. Horvath, M. F. Bruist, M. I. Simon and P. B. Dervan, *Science, 238* (1987) 1129.
17 (a) G. Dougherty and J. R. Pilbrow, *Int. J. Biochem., 16* (1984) 1179; (b) M. Chein, A. P. Grollman and S. B. Horwitz, *Biochemistry, 16* (1977) 3641; (c) L. F. Povirk, M. Hogan, N. Dattagupta and M. Buechner, *Biochemistry, 20* (1981) 665; (d) K. H. Langley, M. R. Patel and M. J. Fournier, in D. B. Satelle, W. I. Lee and B. R. Ware (eds.), *Biomedical Applications of Laser Light Scattering,* Elsevier, Amsterdam, 1982, pp. 37–49.
18 S. J. Brown, P. K. Mascharak and D. W. Stephan, *J. Am. Chem. Soc., 110* (1988) 1996.
19 S. J. Brown, S. E. Hudson, D. W. Stephan and P. K. Mascharak, *Inorg. Chem., 28* (1989) 468.
20 (a) G. McLendon and A. E. Martell, *J. Chem. Soc., Chem. Commun.,* (1975) 223; (b) *Coord. Chem. Rev., 19* (1986) 1; (c), W. R. Harris, I. Murase, J. H. Timmons and A. E. Martell, *Inorg. Chem., 17* (1978) 889; (d) J. H. Timmons, W. R. Harris, I. Murase and A. E. Martell, *Inorg. Chem., 17* (1978) 2193.
21 (a) J. H. Timmons, R. H. Niswander, A. Clearfield and A. E. Martell, *Inorg. Chem., 18* (1979) 2977; (b) J. H. Timmons, A. Clearfield, A. E. Martell and R. H. Niswander, *Inorg. Chem., 18* (1979) 1042.

22 R. Machida, E. Kimura and M. Kodama, *Inorg. Chem., 22* (1983) 2055.
23 E. Kimura, M. Kodama, R. Machida and K. Ishizir, *Inorg. Chem., 21* (1982) 595.
24 N. Herron and D. H. Busch, *J. Am. Chem. Soc., 103* (1981) 1236.
25 (a) J. P. Collman, J. I. Brauman, K. M. Doxsee, J. L. Sessler, R. M. Morris and Q. H. Gibson, *Inorg. Chem., 22* (1983) 1427; (b) J. P. Collman, T. Halbert and K. S. Suslick, in T. G. Spiro (ed.), *Metal Ion Activation of Dioxygen*, Wiley, New York, 1980, Ch. 1.
26 J. Geibel, J. Cannon, D. Campbell and T. G. Traylor, *J. Am. Chem. Soc., 100* (1978) 3575.
27 (a) J.-P. Henichart, J.-L. Bernier, R. Houssin, M. Lohez, A. Kenani and J. P. Latteau, *Biochem. Biophys. Res. Commun;. 126* (1985) 1036; (b) J.-P. Henichart, R. Houssin, J.-L. Bernier and J.-P. Catteau, *J. Chem. Soc., Chem. Commun.*, (1982) 1295.
28 T. J. Lomis, J. F. Siuda and R. E. Shepherd, *J. Chem. Soc., Chem. Commun.*, (1988) 290.
29 T. J. Lomis, M. G. Elliott, S. Siddiqui, M. Moyer, R. R. Koepsel and R. E. Shepherd, *Inorg. Chem., 28* (1989) 2369.
30 T. J. Lomis, J. Martin, B. McCloskey, S. Siddiqui, S. Zhang, R. E. Shepherd and J. F. Siuda, *Inorg. Chim. Acta, 157* (1989) 99.
31 H. Kurosaki, H. Anan and E. Kimura, *Nippon Kagaku Kaishi*, (1988) 691.
32 Y. Iitaka, H. Nakamura, T. Nakatani, Y. Muraoka, A. Fuji, T. Takita and H. Umezawa, *J. Antibiot., 31* (1978) 1070.
33 J. O. Lundgren, *UPALS*, a full matrix least-squares refinement program, Institute for Chemistry, University of Upsala, Sweden, 1978.
34 S. A. Khan and R. P. Novick, *Plasmid, 10* (1983) 251.
35 T. Maniatis, E. F. Fritsch and J. Sambrook, *Molecular Cloning: A Laboratory Manual*, Cold Spring Harbor Laboratory, Cold Spring Harbor, NY, 1982.
36 A. M. Maxam and W. Gilbert, in L. Grossman and K. Moblave (eds.), *Methods in Enzymology*, Vol. 65, Academic Press, New York, 1980, pp. 499–560.
37 H. Sigel and R. B. Martin, *Chem. Rev., 82* (1982) 385.
38 S. J. Brown, X. Tao, D. W. Stephan and P. K. Mascharak, *Inorg. Chem., 25* (1986) 3377.
39 C. K. Johnson, *ORTEP II*, Oak Ridge National Laboratories, Oak Ridge, TN, 1978.
40 W. W. Henderson, R. E. Shepherd and J. Abola, *Inorg. Chem., 25* (1986) 3157.
41 C. R. Johnson, C. M. Jones, S. A. Asher and J. E. Abola, *J. Am. Chem. Soc.*, (1989) submitted for publication.
42 K. T. Potts, *Comprehensive Heterocyclic Chemistry*, Vol. 5, Pergamon, Oxford, 1984, p. 350.
43 M. G. Elliott and R. E. Shepherd, *Transition Met. Chem., 14* (1989) 251.
44 (a) A. J. Gordon and R. A. Ford, *The Chemist's Companion*, Wiley Interscience, New York, 1972, pp. 107–108; (b) L. Pauling, *The Nature of the Chemical Bond*, Cornell Press, Ithaca, NY, 3rd edn., 1960, pp. 281–282; (c) R. Osterberg and B. Sjoberg, *J. Chem. Soc., Chem. Commun.*, (1972) 983; (d) J. F. Blount, K. A. Fraser, H. C. Freeman, J. T. Szymanski and C.-H. Wang, *Acta Crystallogr., 22* (1967) 396; (e) P. D. Meester and D. J. Hodgson, *Acta Crystallogr., Sect. B, 33* (1977) 3505.
45 C. R. Johnson, T. K. Myser and R. E. Shepherd, *Inorg. Chem., 27* (1988) 1089.
46 (a) E. G. Janzen, *Acc. Chem. Res., 4* (1971) 31; (b) C. A. Evans, *Aldrichim. Acta, 12* (1979) 23.
47 L. M. Fisher, R. Kuroda and T. T. Sakai, *Biochemistry, 24* (1985) 3199.